Theoretical, Numerical and Experimental Investigation of a Faraday Disc Generator for Energy Harvesting Applications

Jorge Luis Galván-Ruiz, F. S. Sellschopp-Sanchez, Michel Rivero, Carlos Álvarez-Macías, Raúl A. Ávalos-Zúñiga and Rodrigo Loera-Palomo

***Abstract*—This work investigates theoretically, numerically, and experimentally a Faraday disc generator. A Faraday disc consists of a conducting solid ring-shaped rotates at different speeds while immersed in a magnetic field. Their interaction induces an electric potential difference between the inner and outer radii of the disc, which is measured by connecting a C-shaped load resistor of aluminum. This generator is constructed from readily available, inexpensive materials that can be conveniently replicated in any laboratory. This approach provides an effective educational tool for understanding the underlying physics of electromagnetic induction phenomena, construction challenges, and capabilities this type of small-scale DC generator device offers. Such generators can be used as a starting point for harvesting untapped kinetic energy, such as the movement of the human body and vibrations in machinery, among others. In addition, we discuss the challenge of designing and constructing a load resistance that allows measurement and power generation on the generators in the centimeter scale for energy harvesting applications, aiming to replace batteries for several sub-watt electronic devices.**

***Index Terms* - Faraday disc, electromagnetic induction, energy harvesting, experiment, theoretical analysis**

I. Introduction

The need for efficient and reliable energy harvesting devices has risen in recent years due to the increasing demand for low-power and autonomous devices [1]. The rapid growth of miniaturized electronics, networked smart electronic devices, and the Internet of Things (IoT) [2], [3] requires reliable power sources such as batteries. These imply considerable challenges towards a successful energy transition, particularly in finding new ways to replace batteries, which have technological and environmental concerns. For example, a billion IoT devices that work with batteries imply 274 million battery changes per day [4], [5]. Among the diverse kinetic energy sources, a particular interest exists in that produced by the movement of the human body. Energy harvesting from natural human motion represents a promising alternative to power some portable devices [6]. For example, in Latin America, energy harvesting has been used to quantify the energy potential of mechanical energy from direct contact of a prosthetic foot with the ground when walking [7]. However, one of the main challenges in this field is designing generators that can effectively convert energy harvesting from unusable sources, such as natural human movements or mechanical vibrations products of everyday activities, into electrical power. The human body, as well as a large number of industrial processes and everyday technological applications, are an unlimited source of small amounts of "unused" (sometimes also referred to as *wasted*) energy [8]. Examples of systems that use this energy obtained through different means are the nano-generators [9]. Some types of these generators are mainly based on *piezoelectricity* [10], in which deformations produced by some forcing element, such as footsteps, are used to generate electrical energy; by *triboelectricity* [11], caused by electromagnetic effects generated by the friction of two materials [12]. However, the available energy that can be recovered is in the order of a few milliwatts, requiring specific adaptation.

Several configurations have been proposed for energy harvesting of human motion, including the vortex-type magneto-hydrodynamic generator [13], [14], which can withstand high pressures and aperiodic movement. In this case, the fluid is confined between two electrically conducting concentric cylinders and moves in the azimuthal direction. The whole system is immersed in an axial magnetic field whose values ranged from $139 - 400$ mT. This system leads to complex three-dimensional flows [13] that greatly simplify by considering the fluid an ideal solid electrical conductor performing a rigid rotation. In this case, the system reduces to the Faraday disc generator, which might have different configurations [15]. A Faraday disc generator can be constructed and characterized in the laboratory, and a systematic investigation helps in understanding the underlying phenomena. This is valuable as a starting point toward designing electric power devices and as a teaching resource.

In [16], a Faraday disc generator was analyzed experimentally and theoretically under open circuit conditions. The structure of this work is organized as follows. In Section II, we present the theoretical model for the Faraday disc generator.

J. L. Galván Ruiz, F. S. Sellschopp Sánchez and C. Álvarez Macías: TecNM/I.T. La Laguna, Graduate Studies and Research on Electrical Engineering, 27000, Torreon, Coah, Mexico. e-mail: ssellsch@gmail.com, calvarezm@correo.itlalaguna.edu.mx

M. Rivero: Instituto de Investigaciones en Materiales, Unidad Morelia, Universidad Nacional Autónoma de México, 58190, Morelia, Michoacán, Mexico.

R. A. Ávalos Zúñiga: Centro de Investigación en Ciencia Aplicada y Tecnología Avanzada, Unidad Querétaro, Instituto Politécnico Nacional, 76090 Querétaro, Mexico.

R. Loera Palomo: CONACYT - TecNM/I.T. La Laguna, Graduate Studies and Research on Electrical Engineering, 27000, Torreon, Coah, Mexico.

Next, in Section III, we describe the numerical model and assumptions employed to simulate the problem. In section IV, we provide details of the experimental setup and conditions used for characterizing the generator. We then present and discuss the theoretical, numerical, and experimental results in Section V. Specifically, we analyze the effect of the disc's rotation speed on electrical variables and investigate the external load's effect theoretically. Finally, we offer the concluding remarks in Section VI.

II. Theoretical Model

The system under examination is a ring-shaped solid with an internal radius r_i, an external radius r_o, and a height of H, as shown in Figure 1. The solid is immersed in a uniform axial magnetic field B_0 and rotates at a steady angular velocity ω_0. Thus, the azimuthal velocity is $u_\theta(r) = \omega_0 r$. The interaction between the rotating ring and the applied magnetic field induces an electric potential drop in the radial direction, which can be measured. This corresponds to the classical Faraday disc (see [17], [18]), depicted in Figure 1, conceptualized as a conductive disc with radius r_o that rotates at a tangential velocity $u_\theta(r)$ in a uniform magnetic field $\vec{B} = B_0\hat{z}$. The electromotive force induced by the relative motion of the disc to the magnetic field between an inner radius r_i of the disc and its outer edge at r_o, can be calculated using Faraday's law of induction.

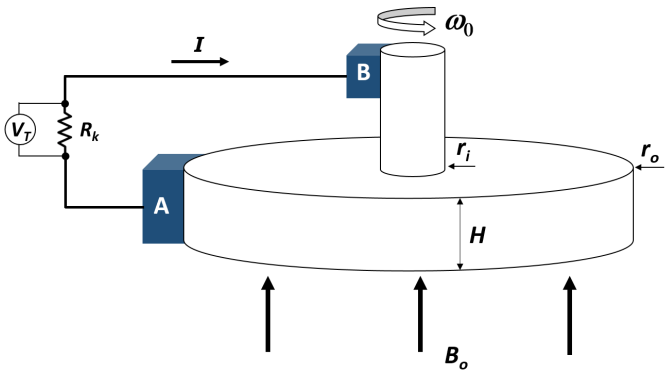

Fig. 1. Homopolar disc generator under a) open circuit conditions, and b) connected to an external electrical load R_k.

In general, Ohm's law for a moving conductor in the laboratory frame of reference states that $\vec{j} = \sigma\left(\vec{E} + \vec{v}\times\vec{B}\right)$, where $\vec{j}$ is the current density flowing in the system and $\vec{E}$ is the electric field associated with a fixed (transformer) or an electrostatic source. Let's assume steady-state (pseudo-static) conditions, implying charge conservation condition $\nabla\cdot\vec{j} = 0$ [13], and take the divergence of both sides of Ohm's law. Therefore, $\nabla\cdot\vec{E} = -\nabla\cdot\left(\vec{v}\times\vec{B}\right)$. Thus, if the divergence of $\vec{v}\times\vec{B}$ is not zero, there exists an electrostatic charge density, ρ_e, which is given by the Gauss's law for an electric field [17] as:

$$\rho_e = -\epsilon_0\epsilon_r\nabla\cdot\left(\vec{v}\times\vec{B}\right) \tag{1}$$

where ϵ_0 and ϵ_r are the electric and dielectric constants respectively. This implies that $\vec{E}$ is not zero and can be calculated from Ohm's law as

$$\vec{E} = -\vec{v}\times\vec{B} + \vec{j}/\sigma \tag{2}$$

For the case of the Faraday disc generator working under open circuit conditions ($R_k \to \infty$ in Figure 1), $\vec{j} = 0$ because no currents can flow between the terminals AB. Under these conditions, the electric field is simplified as:

$$\vec{E} = -\vec{v}\times\vec{B} = -\omega_0 B_0 r\hat{r} \tag{3}$$

which results from separating electrical charges due to the electromagnetic force in the radial direction $\hat{r}$. Note the electric field is a function only of radius r. For a static magnetic field, the differential form of Faraday's law is given as $\nabla\times\vec{E} = 0$, implying that $\vec{E} = -\nabla\phi$, where ϕ is the electric potential. Therefore, the electric potential drop between the inner and outer radii, $\Delta\phi = \phi(r_o) - \phi(r_i)$, that is between terminals AB can be calculated as:

$$\Delta\phi = V_T = -\int_C \vec{E}\cdot d\vec{l} = \int_{r_i}^{r_o} \omega_0 r B_0\, dr \tag{4}$$

where V_T is the voltage between the terminals AB, also known as terminal voltage.

It is important to note that the magnetic field associated with the induced current, $\vec{j}$, has been neglected in relation to the imposed magnetic field B_0. This approach is known as the inductionless approximation [13], and it is valid when induced effects are much lower than the Joule dissipation [19]. Now, let's examine the scenario when the Faraday disc is connected to an external electrical load R_k through sliding contacts (R_k finite in Figure 1). In this case, from $\nabla\cdot\vec{j} = 0$, the current flows radially in the disc in the form of:

$$\vec{j} = \frac{I}{2\pi H}\frac{1}{r}\hat{r} \tag{5}$$

where I is the total current flowing in the circuit. Now the electric field is given as:

$$\vec{E} = \left(-\omega_0 B_0 r + \frac{I}{2\pi H\sigma}\frac{1}{r}\right)\hat{r} \tag{6}$$

containing an additional term if compared to the open circuit case. The electric potential drop between points AB is calculated from the definition given by (4), resulting in:

$$\Delta\phi = \frac{\omega_0 B_0}{2}\left(r_o^2 - r_i^2\right) - \frac{I}{2\pi H\sigma}\ln\left(\frac{r_o}{r_i}\right) \tag{7}$$

or in

$$V_T = V_{oc} - IR_i \tag{8}$$

where $V_{oc} = \omega_0 B_0\left(r_o^2 - r_i^2\right)/2$ is the open circuit voltage and

$$R_i = \frac{\ln(r_o/r_i)}{2\pi\sigma H} \tag{9}$$

is the internal resistance of the ring-shaped solid. Equation (8) is the expression of a non-ideal voltage source [18], as illustrated in Figure 2.

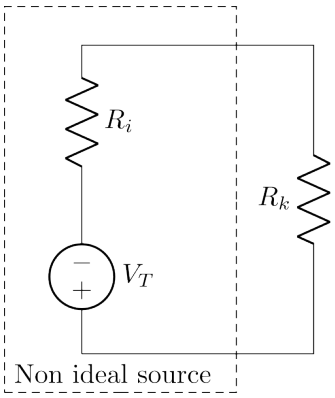

Fig. 2. Non ideal voltage source diagram, with R_i is the internal resistance of the disc and R_k the load resistance.

To calculate the terminal voltage V_T, we replace $I = V_T/R_k$ in equation (8) and solve for V_T. This results in

$$V_T = V_{oc}K \tag{10}$$

where $K = R_k/(R_i + R_k)$ is defined as the load factor. Similarly, an expression for the total current can be derived, which results in

$$I = \frac{V_{oc}}{R_i}(1 - K) \tag{11}$$

The overall electrical power is then

$$P_e = V_T I = \frac{V_{oc}^2}{R_i}(1 - K)K \tag{12}$$

According to (12), the maximum electrical power transfer occurs when $K = 1/2$, indicating that the external resistance equals the internal resistance of the system.

III. Numerical model

A numerical model was implemented to simulate the generator using the COMSOL Multiphysics software [20]. From the AC/DC module, the Magnetic fields without currents, Electric currents, and Electric circuits sub-modules were employed. Three distinct domains were constructed: the aluminum disc, cylindrical neodymium permanent magnet (N35 grade, with a diameter of 50 mm and height of 10 mm), and the air (a cubic volume containing all domains). The external resistance is modeled by the Electric Circuit sub-module, in whose case only the measured value is required. The magnet and disc are concentrically located and separated by a given distance. According to the experimental setup, the parameters used for simulations are shown later in Table I. To avoid using deformable or sliding meshes, a tangential velocity was imposed on the disc to simulate its rotation (prescribed velocity field), enabling a static mesh. For the magnetic field, walls are placed far enough to apply a zero magnetic field at these boundaries. The equations solved in the AC/DC module are Ampere's and Ohm's laws, as shown:

$$\frac{1}{\mu_0}\nabla \times \vec{B} = \vec{j} = \sigma\left(\vec{E} + \vec{u} \times \vec{B}\right) \tag{13}$$

as well as the condition of charge conservation $\nabla \cdot \vec{j} = 0$. In the software, the electric scalar potential ϕ and the magnetic potential vector $\vec{A}$ are used as primary variables, allowing the magnetic and electric fields to be expressed in relation to these variables. Specifically, $\vec{B} = \nabla \times \vec{A}$ and $\vec{E} = -\nabla\phi - \frac{\partial \vec{A}}{\partial t}$. As a result, Ampere's and Ohm's laws can be rewritten as:

$$\nabla \times \left(\frac{1}{\mu_0}\nabla \times \vec{A}\right) + \sigma(\nabla\phi - \vec{u} \times (\nabla \times \vec{A})) = 0 \tag{14}$$

$$\nabla \cdot \left(\sigma\nabla\phi - \sigma\vec{u} \times \left(\nabla \times \vec{A}\right)\right) = 0 \tag{15}$$

Note that this analysis assumed a static magnetic field (inductionless approximation) independent of the velocity field. The sequence used to solve the equations was as follows: first, the magnetic field was solved in all domains, considering a zero magnetic field at the outermost boundaries of the proposed working space. Secondly, the velocity, induced electric currents, and electrical circuit modules in the aluminum disc domain were solved.

IV. Experimental setup

We built a Faraday disc generator using readily available and inexpensive materials. The setup can be conveniently replicated in any laboratory, making it an effective tool for educational purposes. The experimental setup consists of a rotating aluminum disc within a magnetic field, as illustrated in Figure 3. The disc, located in front of the magnet, is powered by a 12 V dc motor. The disc is attached to a rigid nylamid coupling, which electrically isolates it from the aluminum shaft (1.9 cm in diameter and 35 cm in length). The magnetic field is generated by a disc-shaped permanent magnet, magnetized in the axial direction, securely fixed to a static nylamid support, and placed at a specific distance from the disc. The shaft, magnet, and disc are aligned along the axis, and the system is mounted on a plywood base. A C-shaped aluminum resistor was constructed to evaluate the generator's response under electrical load conditions. The resistance cross-section decreases at both ends to contact the disc's internal and external radii (see Figure 3), allowing it to make contact with the aluminum disc's terminals.

Figure 3 illustrates the experimental setup, including the disc, magnet, optical rotation sensor, and the constructed load resistor. A CC Agilent/Keysight E3632A voltage source was used to power the dc motor and rotate the disc at the desired speed. The dc motor enables rotation speeds ranging from 928 to 1635 RPM. The magnetic flux intensity at 2.6 mm from the magnet's surface was measured with *Tesla Meter WT10A Gaussmeter Surface Magnetic Field Tester*. This value was used to calibrate the numerical model. The dimensions and physical properties of the disc, magnet, and of other components are given in Table I.

A. Experimental Characterization

The experimental stage involves driving the Faraday disc at different speeds to measure the induced current between the internal and external radii of the disc when a load resistor is connected. Disc rotation was characterized by an optical rotational sensor mounted on the shaft. As depicted in Figure 3, a clamp-type ammeter measured the electric current.

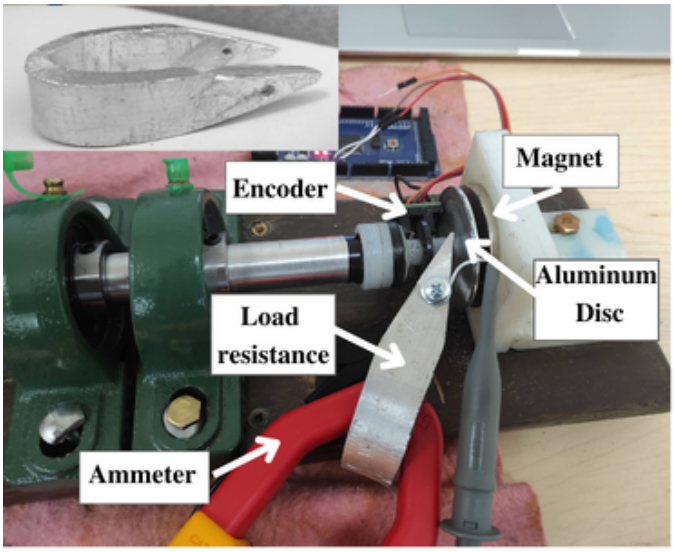

Fig. 3. Picture of the experimental configuration during electrical characterization. The C-shaped aluminum resistor is shown in the inset

TABLE I
MAIN PHYSICAL AND GEOMETRICAL PARAMETERS

	Parameter	value
Disc	Material	Aluminum
	Inner radius	r_i = 2.5 mm
	Outer radius	r_o = 25 mm
	Height	H = 2 mm
	Electrical conductivity σ	37.8×10^6 S m^{-1}
	Rotation speed	$928 - 1635$ RPM
Magnet	Cylindrical ($r \times H$)	25.4×10 mm
	Remanent flux density	1.35 T
	Separation from disc	2.6 mm
Air	Cubic domain	L = 200 mm
	Relative magnetic permeability	1
Load resistance	Material	Aluminum
	Lenght	180 mm
	Height	19.05mm
	Thickness	6.35 mm
	Electrical conductivity σ	37.8×10^6 S m^{-1}

1) Rotational speed measure: A 20-segment digital optical sensor LM6490 connected to the aluminum shaft and an Arduino board was used to read and record the sensor data. Each reported measurement corresponds to average values.

2) Induced current: The induced current in the generator under loaded conditions was measured using a Fluke POWER CLAMP 345-PQ clamp ammeter. The current flowing through the load resistor was measured, as depicted in Figure 3, utilizing the instrument's ability to measure using the Hall effect. The obtained values were processed by calculating the averages and standard deviations.

When using the Hall effect to measure the current flowing through the load, it is essential to consider the magnetic field generated by the flowing current. Since the resistor is close to the permanent magnet, its magnetic field interferes with the current measurements of interest. Namely, as the ammeter detects the permanent magnet, a constant electrical current was measured at a fixed position, the reference current. This way, the reference current (no rotation) was subtracted from the total current values obtained while the generator was operating, leaving only the electric current values induced by the rotation.

V. RESULTS AND DISCUSSION

This section compares the results obtained from the experimental, numerical, and analytical models. The average values of the induced currents and the discrepancies are also validated and discussed. The variables obtained from the experimentation, such as the average speeds and the physical characteristics of the experiment (I), were utilized in the analytical and numerical models to compare the results of all of them.

A. Experimental Results

The experimental setup, described in Section IV, was tested at four rotating speeds: 928, 1299, 1422, and 1635 RPM while a load resistor was connected between the terminals. The magnet, disc, and separation were the same throughout all experiments; thus, the non-uniform magnetic field distribution was identical. Measurements were carried out for each rotation speed during $2 - 3$ minutes of steady-state operation. These measurements consider the rotation speed and the total current when the electric load is connected. The reported values of both variables correspond to the average of the experiment duration. The reference current was measured before each experiment. It's worth mentioning that another relevant variable of the experimental model is the load resistance, and its construction and characterization play a crucial role in this research.

1) Load resistance: The internal resistance of the aluminum disk, computed from (9), is $R_i = 4.84\ \mu\Omega$. The maximum power output is obtained when the external load is equal to the internal resistance [13], namely, $R_K = R_i$. So, for the aluminum disc of 25 mm radius, building a load resistor with such a resistance value is not an easy task. Let us estimate the cross-section of this resistor, considering a cylindrical geometry (wire), which can be carried out using the following equation:

$$R_k = \rho \frac{l}{A} \tag{16}$$

where R_k is the load resistance, ρ is resistivity, l is length, and A is the transversal area. From (16), we can solve for the radius once all other variables are defined. For $R_k = R_i$, a 10 cm long wire, the radii would be 21.71 mm and 17.52 mm for aluminum and copper wires, respectively. Namely, it would require more space than the length and area of the aluminum disc of the Faraday disk, making them non-viable options for the resistor, because it must be connected to the internal and external radius of the disk. Reasonable wire diameters (0.68 mm for aluminum and 0.55 mm for copper) are obtained for a thousand times bigger resistance ($R_k = 4.84$ mΩ). These are schematized in Figure 4. Consequently, a resistor in the mΩ scale is a feasible option for experimentation, even if this

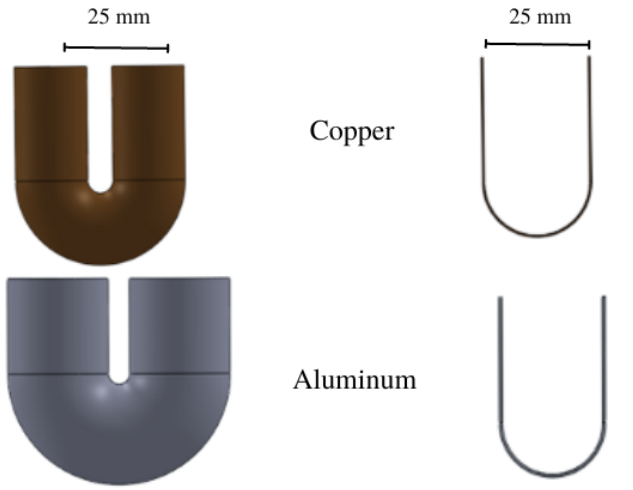

Fig. 4. Schemes of the load resistor sizes with *left*) $R_k = R_i = 4.84\ \mu\Omega$ and *right*) $R_k = R_i = 4.84$ mΩ.

leads to much lower power, that can be used to investigate the generator with the load resistance.

The final design of the resistor, shown in Figure 3b), consists of a rectangular bar with long end tips on both extremes. The resistor's electrical current streamlines (see Figure 5) were simulated with COMSOL Multiphysics. During experimentation, it was observed that the friction between the rotating disc and the static terminals of the resistor caused wear on both tips, which ultimately affected its internal resistance. As established in (9), the total resistance of a conductor is inversely proportional to its cross-sectional area, so when wear occurs at the tips, this area increases, and the load resistance decreases.

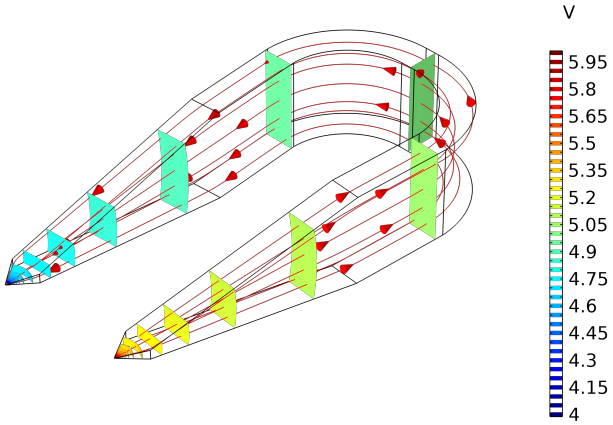

Fig. 5. Resistor's electrical current streamlines in red and isosurfaces of the electric potential. Numerical results from COMSOL simulations

Experiments showed that despite minimal resistor wear, it significantly affects the overall electrical variables due to the change in its internal resistance. A direct physical measurement of the wear length (ℓ) during experimentation is challenging, and this research does not intend to cover frictional wear resistance in this way. A simulation of this resistance for different wear lengths was performed to investigate this effect. In this case, a constant voltage was applied on both ends to observe how its internal resistance varies. Figure 6 shows the load resistance as a function of the wear length. In this case, the internal resistance decays as $R_k = 0.2329\ \ell^{-0.922} (R^2 = 0.9992)$. This plot shows the impact of a minimum wear length in which a slight increase in wear lead to a significant decrease in the resistance for wear lengths below 0.2 mm, representing a 73% drop in its value. Coincidently, these significant variations correspond to the cases observed experimentally, which must be considered for generator analysis.

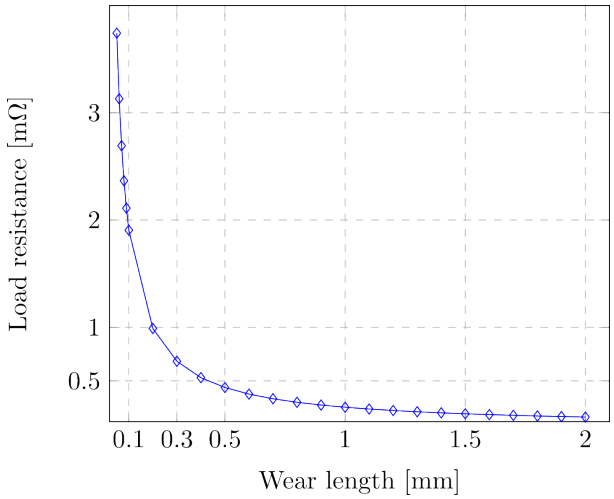

Fig. 6. Resistance as a function of the wear length. Numerical results from COMSOL simulations

2) Experimental induced current: Induced electric current flowing just through the load was measured for different rotation speeds, and their average values and standard deviation are shown in Figure 7. The error bars correspond to one standard deviation for each case. As observed, the induced current increases monotonically with the rotation frequency, as expected from the analytical model. Note that the standard deviation also increases with the rotation speed. This can be attributed to i) the load resistance variation during the experiments due to wearing, leading to larger uncertainties in the measurements, and ii) possible mechanical vibrations and misalignment of the components. In addition, it is noteworthy that wearing the resistor is faster for higher speeds, which contributes to the uncertainty.

Since the voltage was not measured during experiments, it can be estimated from Ohm's law, $V = IR$. From this law, the voltage exhibits the same behavior as the current. For this purpose, the resistance was measured during all experiments, in which we noticed wearing in the tips. Resistance measurements were performed with the Keithley 2120-100 digital multimeter using the 4-point technique. In our case, the resistance values stood in the range of $1 - 10$ mΩ, consistent with the numerical simulation presented in the previous section (see Figure 6). Therefore, given the uncertainty in resistance and current, we obtain a range of values instead of getting a single voltage value for each speed. This is presented in

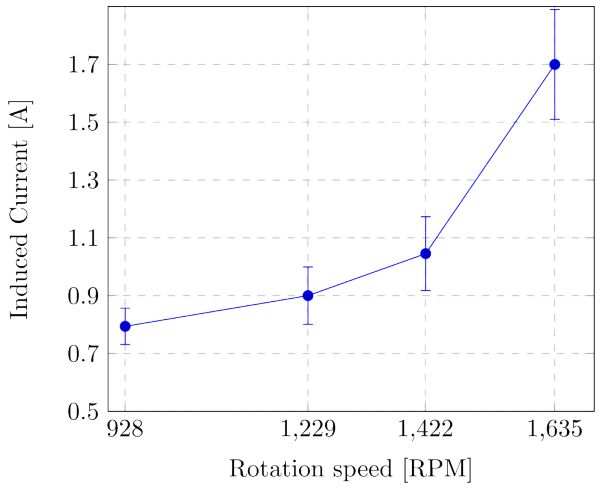

Fig. 7. Measured induced current as a function of the rotation speed

Figure 8. The curve limits, ranging from 1 mV to 17 mV for the different speeds, are obtained from the lowest and highest resistance and current values.

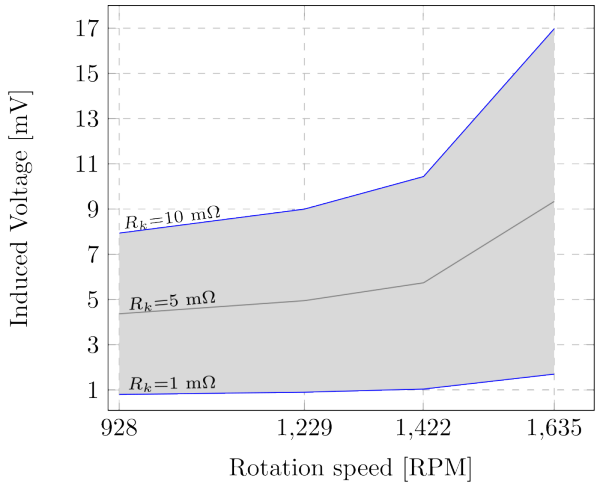

Fig. 8. Calculated induced voltage as a function of rotation speed considering a load resistance ranging from 1 mΩ $< R_k <$ 10 mΩ (shaded area)

The electric power can be computed readily from the measured total electric current and estimated voltage, $P_e = I\ V_T$. This is shown in Figure 9. The electric power of the Faraday disc under load conditions exhibits a behavior similar to electric current and voltage with respect to the rotation speed. For the explored experimental conditions, the estimated power varied from 0.5 mW at 928 RPM (lower bound) to 28 mW at 1635 RPM (upper bound). It is important to note that the load resistance is three orders of magnitude higher than the internal resistance of the disc. Thus, a higher power output can be achieved if the experimental setup is optimized, which is out of the scope of the present work.

B. Theoretical Results

In this section, the analytical (Section II) and numerical (Section III) models are discussed and compared with the

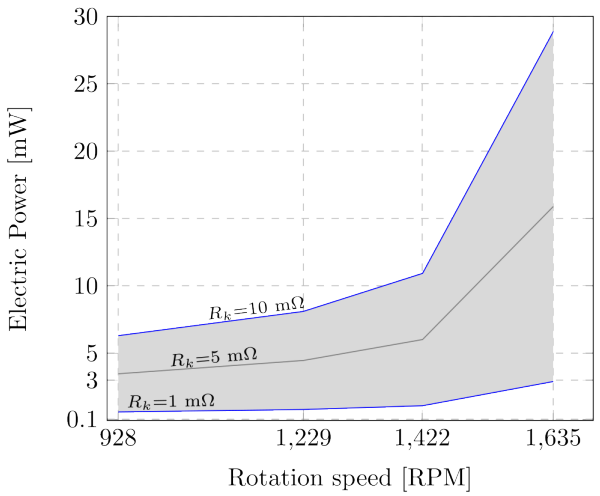

Fig. 9. Electric power as a function of rotation speed considering a load resistance ranging from 1 mΩ $< R_k <$ 10 mΩ (shaded area)

experimental results presented in the previous section. For this purpose, the physical and geometrical parameters (see Table I), as well as the average load resistances for the corresponding rotation speeds, are considered for both theoretical models. Moreover, for visualization, the magnetic flux density and electric current field obtained from the numerical model are presented in Figure 10. The average magnetic flux density in the disc domain was found to be 196 mT.

The validation of the two theoretical models with experimental results is based on the measured induced current, as well as the estimated voltage and electric power under load conditions. Figure 11 shows the induced current obtained experimentally and the values obtained from the analytical and numerical models. The results show a good agreement between the analytical and numerical models, with an error percentage of approximately 2.3%. It is important to note that theoretical and experimental results show an acceptable agreement (within the same order of magnitude), despite the simplification of the theoretical models and the systematic errors in the experimental characterization, which lead to error percentages ranging from $18 - 43\%$. This difference could be attributed to the following assumptions or experimental limitations: disregarding the contact (frictional) resistance and nutation of the rotating disc, the methodology for determining the induced current, and the resistance wear that may result in load resistance variations during characterization. Although possible misalignments and vibrations could affect the experimental results, based on our observations, the uncertainty source is the frictional resistance. A feasible solution to this late issue is to use liquid metals to ensure electrical contact [21], which could also prevent the wearing of the parts. However, the compatibility of the materials must be ensured.

The comparison of results for the induced voltage and output power are presented in Figures 12 and 13, respectively. As for the induced current, a similar comparison is observed among the models. Moreover, estimated values are in the same order of magnitude as the theoretical ones. Nevertheless, the induced voltage from the theoretical models is within the

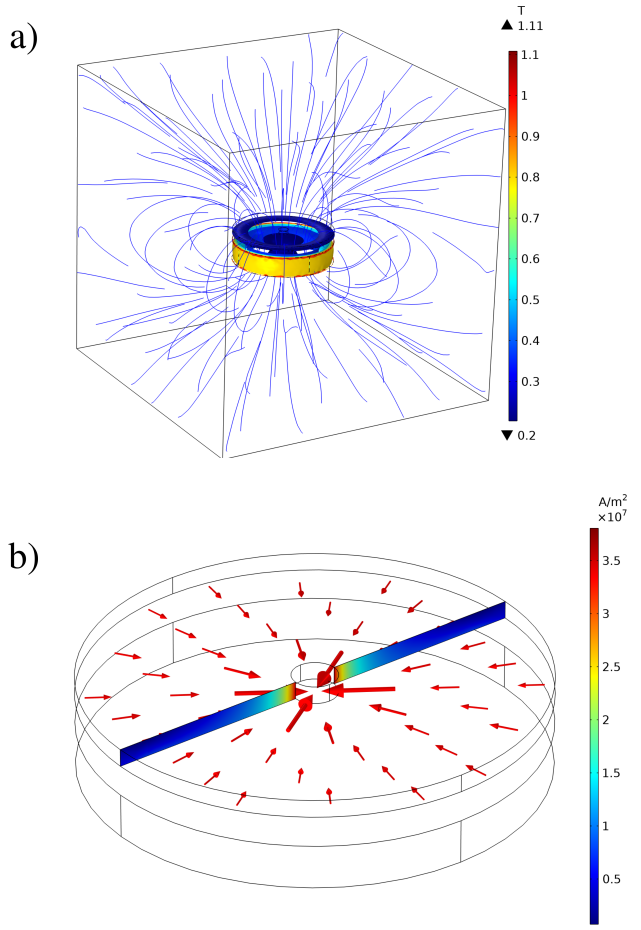

Fig. 10. a) Streamlines of the magnetic flux density (in T), and b) electric current field and voltage isosurfaces. Numerical results

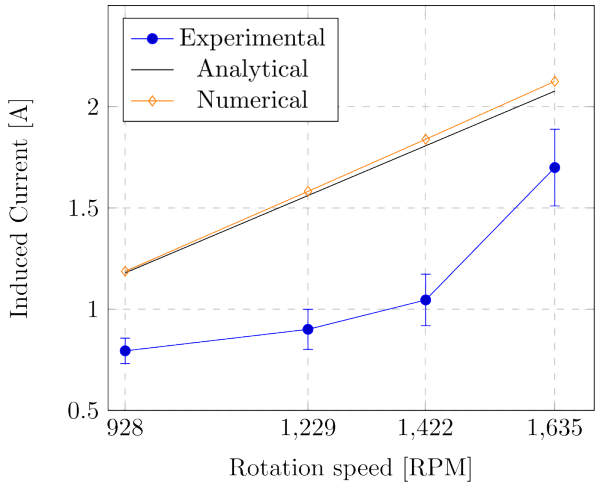

Fig. 11. Induced current as a function of rotation speed for experimental (see Fig. 7), analytical, and numerical models.

calculated values, while the output power agrees it only occurs at the higher rotation speed. Since these values are derived from the induced current, discrepancies among models can be explained by the same arguments. Smaller errors are expected if the uncertainty in determining the load resistance is reduced, and systematic errors in measuring the induced current are avoided.

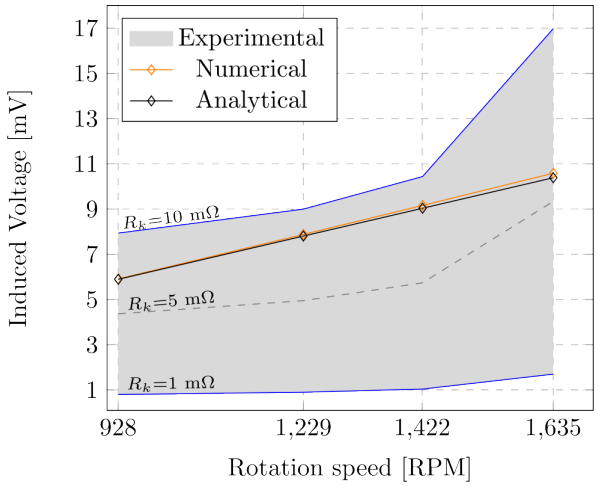

Fig. 12. Induced voltage as a function of a rotation speed for the experimental (1 mΩ $< R_k <$ 10 mΩ), analytical, and numerical models

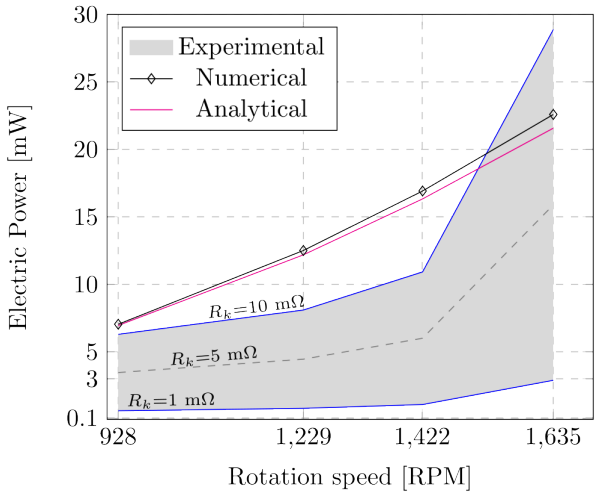

Fig. 13. Electric power as a function of rotation speed experimental (1 mΩ $< R_k <$ 10 mΩ), analytical, and numerical models

Although the theoretical models show a good agreement with experimental results and are prone to be improved, the approach described in this work to investigate a Faraday disc generator is of great interest for educational purposes. The experimental setup presented here is suitable for use in school laboratories to systematically investigate the impact of different variables on the system. As for the experimental results, the construction and characterization of the load resistance and the technique used for the electrical characterization of the system are the main contributions of this model. Estimating an appropriate load resistance that matches the internal resistance of the device is a complex task, as discussed in the results section, and will be further investigated. Although the analysis of load sizing has already been presented in this paper, it serves as a reference for future experimentation.

VI. Conclusions

This work investigates a Faraday disc analytically, numerically, and experimentally. The experiments were conducted with a 50 mm diameter and 2 mm height aluminum disc rotating ($928-1635$ RPM) immersed in a stationary magnetic field. We measured the induced total current, and the induced voltage and output power were estimated using the measured load resistance and electric current. The geometrical and physical parameters restricted the minimum reachable resistance to the order of some mΩ. The numerical and analytical models are in good agreement but present a fair agreement with experimental results. Although all results are within the same range of values, experimental results exhibited non-linear behavior with the rotation speed. According to observations, this non linearity can be attributed to the modification of the electrical resistance of the external load because of wearing (which is found to be significant), disregarding contact resistance, vibration or misalignment of the rotating parts, and the proposed methodology to determine the induced current. All these aspects are prone to be diminished.

This work provides a methodology to build and characterize a Faraday disc, which helps understand the phenomena of electricity generation that can be scaled to small geometries aiming to low power consumption (in the sub-watt scale) electronics. The experimental setup described in this study can be easily replicated in school laboratories, providing an accessible platform to explore the effects of various parameters on the system's performance. This configuration allows for a comprehensive investigation of key factors such as conductivity, magnetic flux density, and geometrical variables, providing a valuable opportunity for students and researchers to gain hands-on experience and develop a deeper understanding of the system. As such, this setup has the potential to enhance science education and promote innovation in related fields.

Acknowledgment

The authors thank Cesar Alberto Hernández Jacobo for his technical support in the experimental implementation. M. Rivero acknowledges UNAM-DGAPA-PAPIIT Project IA100621.

References

[1] Y. Mao, G. Yu, and C. Zhong, "Energy consumption analysis of energy harvesting systems with power grid," *IEEE Wireless Communications Letters*, vol. 2, no. 6, pp. 611–614, 2013.

[2] T. Hiramoto, K. Takeuchi, T. Mizutani, A. Ueda, T. Saraya, M. Kobayashi, Y. Yamamoto, H. Makiyama, T. Yamashita, H. Oda, S. Kamohara, N. Sugii, and Y. Yamaguchi, "Ultra-low power and ultra-low voltage devices and circuits for IoT applications," in *2016 IEEE Silicon Nanoelectronics Workshop (SNW)*, pp. 146–147, 2016.

[3] C. M. Medina Otalvaro, J. C. Blandón Andrade, C. M. Zapata Jaramillo, and J. I. RiosPatiño, "IoT best practices and their components: A systematic literature review," *IEEE Latin America Transactions*, vol. 20, p. 2217–2228, Jul. 2022.

[4] S. Khalid, I. Raouf, A. Khan, N. Kim, and H. S. Kim, "A review of human-powered energy harvesting for smart electronics: Recent progress and challenges," *International Journal of Precision Engineering and Manufacturing-Green Technology*, vol. 6, pp. 821–851, 2019.

[5] M. Alhawari, B. Mohammad, H. Saleh, and M. Ismail, *Energy harvesting for self-powered wearable devices*. Springer, 2018.

[6] R. Riemer and A. Shapiro, "Biomechanical energy harvesting from human motion: theory, state of the art, design guidelines, and future directions," *Journal of NeuroEngineering and Rehabilitation*, vol. 8, p. 22, 2011.

[7] D. dos Santos Oliveira and S. d. S. Rodrigues Fleury Rosa, "Analysis of energy harvesting in a new prosthetic foot via bond graph method," *IEEE Latin America Transactions*, vol. 16, no. 12, pp. 2857–2863, 2018.

[8] L. B. Kong, T. Li, H. H. Hng, F. Boey, T. Zhang, and S. Li, "Waste energy harvesting," *Lecture Notes in Energy*, vol. 24, pp. 263–403, 2014.

[9] T. Kaźmierski and S. Beeby, *Energy Harvesting Systems: Principles, Modeling and Applications*. SpringerLink : Bücher, Springer New York, 2010.

[10] A. Jbaily and R. W. Yeung, "Piezoelectric devices for ocean energy: a brief survey," *Journal of Ocean Engineering and Marine Energy*, vol. 1, no. 1, pp. 101–118, 2015.

[11] F.-R. Fan, Z.-Q. Tian, and Z. L. Wang], "Flexible triboelectric generator," *Nano Energy*, vol. 1, no. 2, pp. 328 – 334, 2012.

[12] M. Mariello, F. Guido, V. Mastronardi, M. Todaro, D. Desmaële, and M. D. Vittorio], "Nanogenerators for harvesting mechanical energy conveyed by liquids," *Nano Energy*, vol. 57, pp. 141 – 156, 2019.

[13] R. A. Ávalos Zúñiga and M. Rivero, "Theoretical modeling of a vortex-type liquid metal MHD generator for energy harvesting applications," *Sustainable Energy Technologies and Assessments*, vol. 52, p. 102056, 2022.

[14] M. Rivero, R. A. Ávalos Zúñiga, and S. Cuevas, "A liquid metal MHD vortex generator for energy harvesting applications," *Magnetohydrodynamics*, vol. 58, no. 4, pp. 339–347, 2022.

[15] C. Baumgärtel and S. Maher, "Resolving the paradox of unipolar induction: new experimental evidence on the influence of the test circuit," *Scientific Reports*, vol. 12, p. 16791, 2022.

[16] J. L. Galvan-Ruiz, F. S. Sellschopp-Sanchez, C. Álvarez Macías, R. Lo-era, R. A. Ávalos Zúñiga, and M. Rivero, "Theoretical and experimental investigation of a Faraday disc generator," in *2022 IEEE International Autumn Meeting on Power, Electronics and Computing (ROPEC)*, vol. 6, pp. 1–6, 2022.

[17] P. Lorrain, "Electrostatic charges in $\mathbf{v} \times \mathbf{B}$ fields: the faraday disk and the rotating sphere," *European Journal of Physics*, vol. 11, p. 94, mar 1990.

[18] F. A. Reich and W. H. Müller, "Examination of electromagnetic powers with the example of a faraday disc dynamo," *Continuum Mechanics and Thermodynamics*, vol. 30, pp. 861–877, 2018.

[19] P. A. Davidson, *An Introduction to Magnetohydrodynamics*. Cambridge Texts in Applied Mathematics, Cambridge University Press, 2001.

[20] "COMSOL Multiphysics 6.0." www.comsol.com, 2023.

[21] R. Ávalos and J. Pride, "Realization of bullard's disc dynamo," *Proceedings of the Royal Society A*, vol. 479, 2023.

Jorge Luis Galván Ruiz received his B.S. degree in Mechatronics Engineering and his M.S. degree in Electrical Engineering from the Instituto Tecnológico de la Laguna, Torreón, Mexico, in 2017 and 2020, respectively. He is currently pursuing a Ph.D. degree in Electrical Engineering at the same institution. His current research interests include electrical generation for energy harvesting applications.

F.S. Sellschopp-Sánchez received his B.Sc in Electrical Engineering from the TecNM/Instituto Tecnológico de Tepic in 1994. He received the degree of M.Sc. in Electrical Engineering in 1999 at the TecNM/Instituto Tecnológico de La Laguna and the degree of Doctor of Science in Electrical Engineering at the same institute in 2003. He is a full-time professor at the TecNM/Instituto Tecnológico de La Laguna and his current research areas are electrical machines and power systems applied to the analysis of the power quality and energy efficiency, renewable energy, generation and integration to electrical grids.

Michel Rivero received his B.S. degree in Mechanical Engineering from the National Polytechnic Institute of Mexico, Mexico City, Mexico, in 2004; and his M.S. and Ph.D. degrees in Engineering from the National Autonomous University of Mexico, Mexico City, Mexico, in 2008 and 2012, respectively. From 2012 to 2014, he was a Research Assistant at the Ilmenau University of Technology, Ilmenau, Germany; and from 2014 to 2019, he was a CONACYT Research Fellow at the InstitutoTecnológico de La Laguna, Torreón, Mexico. In 2019, he joined the Instituto de Investigaciones en Materiales, Universidad Nacional Autónoma de México (UNAM), Morelia, Mexico, where he is presently working as an Associate Researcher. His current research interests include renewable energy, magnetohydrodynamics, and thermal energy storage and harvesting.

Carlos Álvarez-Macías is a Senior Research Professor at the Division of Postgraduate Studies and Research from TecNM/La Laguna Institute of Technology at the City of Torreón in Coahuila México since 2016. He's a Physics from the Faculty of Sciences at the National Autonomous University of Mexico (UNAM). He has a Master of Science in Microelectronics from the National Institute of Optics and Electronics (INAOE). He is PhD in Materials Science and Engineering from the materials research institute of the UNAM. With more than 25 scientific publications of international prestige, Dr Álvarez has experience optimizing photovoltaic materials, devices, and systems. His areas of expertise include Nanotechnology applied to Solar Energy. He has been a member of his country's National Solar Energy Association (ANES), the International Solar Energy Society (ISES) and the National System of Researchers, level I. He is currently responsible for the academic body registered in PRODEP and President of the Academy of Renewable Energy Engineering in his institution.

Raúl A. Ávalos Zúñiga completed his bachelor s at the Universidad Autónoma Metropolitana (UAM), Unidad Iztapalapa (1993-1998, Energy Engineering). From 1999-2001 he completed a Master's Degree in Solar Photo-Thermal Energy at the Institute of Renewable Energies (IER) of the National Autonomous University of Mexico (UNAM), and later his Ph.D. at the National Polytechnic Institute of Grenoble (INP Grenoble), in France (2001-2005, in Energy Physics). From 2005-2006 he did a postdoctoral fellowship at the Helmholtz-Zentrum Dresden-Rossendorf Research Center (HZDR), Dresden, Germany. From 2006-2008 he worked as a professor-researcher at the UAM, Iztapalapa Unit, and from 2009-2011 at the Autonomous University of San Luis Potosí. From 2011 to date, he has worked as a professor-researcher in Alternative Energies of the Center for Research in Applied Science and Advanced Technology unit Querétaro (CICATA-Qro) of the National Polytechnic Institute (IPN). He is a member of the National System of Level I Researchers. His research topics include alternative energies and liquid metal magnetohydrodynamics.

Rodrigo Loera-Palomo received his M.S. and Ph.D. degrees in Electrical Engineering from Universidad Autónoma de San Luis Potosí, San Luis Potosí, México, in 2007 and 2013, respectively. He is presently working as a Professor in the Instituto Tecnológico de la Laguna, Torreón, Mexico, through the Cátedras-CONACYT program. His current research interest include power electronics systems, switching converters, and DC-DC power supplies.